

# Free-standing kinked nanowire transistor probes for targeted intracellular recording in three dimensions

Quan Qing<sup>1†</sup>, Zhe Jiang<sup>1†</sup>, Lin Xu<sup>1,2</sup>, Ruixuan Gao<sup>1</sup>, Liqiang Mai<sup>2</sup> and Charles M. Lieber<sup>1,2,3\*</sup>

**Recording intracellular (IC) bioelectrical signals is central to understanding the fundamental behaviour of cells and cell networks in, for example, neural and cardiac systems<sup>1–4</sup>. The standard tool for IC recording, the patch-clamp micropipette<sup>5</sup> is applied widely, yet remains limited in terms of reducing the tip size, the ability to reuse the pipette<sup>5</sup> and ion exchange with the cytoplasm<sup>6</sup>. Recent efforts have been directed towards developing new chip-based tools<sup>1–4,7–13</sup>, including micro-to-nanoscale metal pillars<sup>7–9</sup>, transistor-based kinked nanowires<sup>10,11</sup> and nanotube devices<sup>12,13</sup>. These nanoscale tools are interesting with respect to chip-based multiplexing, but, so far, preclude targeted recording from specific cell regions and/or subcellular structures. Here we overcome this limitation in a general manner by fabricating free-standing probes in which a kinked silicon nanowire with an encoded field-effect transistor detector serves as the tip end. These probes can be manipulated in three dimensions within a standard microscope to target specific cells or cell regions, and record stable full-amplitude IC action potentials from different targeted cells without the need to clean or change the tip. Simultaneous measurements from the same cell made with free-standing nanowire and patch-clamp probes show that the same action potential amplitude and temporal properties are recorded without corrections to the raw nanowire signal. In addition, we demonstrate real-time monitoring of changes in the action potential as different ion-channel blockers are applied to cells, and multiplexed recording from cells by independent manipulation of two free-standing nanowire probes.**

Separation of a nanoelectronic detector element from much larger interconnections is necessary for internalization of the detector without damaging the cell of interest<sup>1–3,10</sup>. To date, all approaches<sup>7–14</sup> have focused on fabricating nanodevices on planar substrates, where the detector protrudes from the surface and target cells are brought into contact with the nanodevices by direct seeding and culture<sup>7–9,14</sup> or manipulation of a culture substrate<sup>10–13</sup> (Fig. 1a). These studies enabled the demonstration of new nanodevice concepts and multiplexed detection, but also have limitations, including (1) device positions are determined during chip fabrication and cannot be reconfigured during an experiment, (2) it is difficult to target specific cells or subcellular regions and (3) minimally invasive *in vivo* measurements are difficult. In comparison, a free-standing probe that can be manipulated in three dimensions (3D; Fig. 1b) would allow targeting of specific cells cultured on substrates or within tissue, although the size of manipulator for such

probes will limit multiplexing compared to chip-based methods<sup>2,3</sup>. In this regard, development of a general strategy to present nanoelectronic device elements, such as the kinked silicon nanowire field-effect transistor (nanoFET)<sup>10</sup>, in a free-standing probe structure could expand substantially the capabilities and applications of these devices in electrophysiology.

The realization of free-standing probes with nanoelectronic device tips requires bridging length scales from the nanoscopic to the macroscopic in a manner that yields robust electrical and mechanical properties. We focus on meeting these challenges for kinked silicon nanowire nanoFET tips as a general example of a two-terminal active nanoelectronic device. In this case, the nanowire arms of the kinked structure serve as nanoscale connections that must be electrically and mechanically connected to the macroscopic handle that serves as input/output to measurement electronics. Our free-standing kinked nanowire probe fabrication involves two overall stages (Fig. 2): (1) lithographic patterning of a nanometre-to-millimetre probe end and (2) mechanical assembly of the probe end to a millimetre-to-macroscopic probe body.

Key steps in the probe-end fabrication are as follows (Fig. 2a–c, Supplementary Methods). First, kinked Si nanowires with nanoFETs encoded synthetically at the kink tip<sup>15</sup> were deposited selectively on a substrate coated with sacrificial nickel and SU8 photoresist layers (Fig. 2a). A representative optical image (Fig. 2d) shows the resulting kinked nanowire and lithography alignment markers. Second, electron-beam lithography (EBL) and photolithography (PL) were used to define the kinked nanowire tip region and the probe body in the SU8 layer, respectively (Fig. 2b). Figure 2e shows the kinked nanowire region after these steps. Metal interconnects and top SU8 passivations were fabricated,

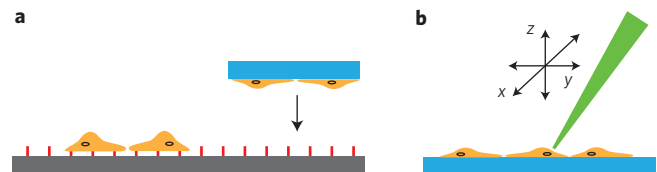


**Figure 1 | Intracellular recording methods.** **a**, Schematic (side view) of a typical recording approach using chip-based device arrays (red) anchored on a planar substrate (grey). Cells (yellow) are usually cultured directly on top of the devices or on a separate substrate (blue), which would be moved into contact with the devices. **b**, Schematic of a free-standing probe, where the probe (green) moves freely in 3D space to target selected cells and/or cell regions.

<sup>1</sup>Department of Chemistry and Chemical Biology, Harvard University, Cambridge, Massachusetts 02138, USA, <sup>2</sup>State Key Laboratory of Advanced Technology for Materials Synthesis and Processing, WUT-Harvard Joint Nano Key Laboratory, Wuhan University of Technology, Wuhan 430070, China, <sup>3</sup>School of Engineering and Applied Sciences, Harvard University, Cambridge, Massachusetts 02138, USA; <sup>†</sup>These authors contributed equally to this work. \*e-mail: cml@cmliris.harvard.edu

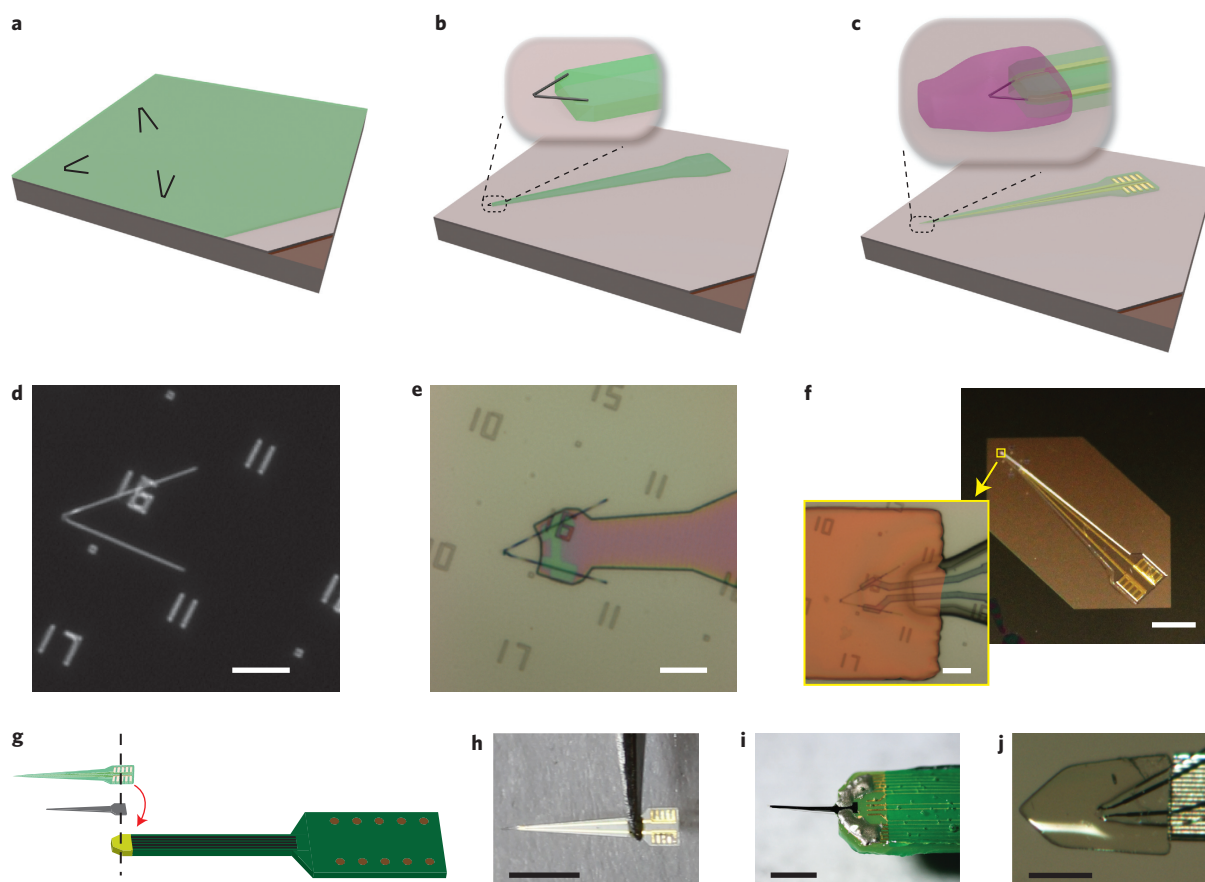


**Figure 2 | Fabrication and assembly of free-standing nanowire probes.** **a**, Si substrate with 600 nm SiO<sub>2</sub> on the surface (brown) coated with a Ni sacrificial layer (pink) and a SU8 polymer layer (light green), and showing deposited kinked silicon nanowires (black). **b**, A kinked nanowire with the desired orientation was identified and fixed on the substrate by EBL (inset), and the bottom structure/passivation layer for the full probe body (light green) was defined by PL. **c**, Metal connections (golden) from the nanowire to the macroscopic contact pads and top passivation layers were fabricated by EBL and PL steps (light green), and then the nanowire was protected by an additional photoresist cap (inset, pink). **d**, Dark-field optical image showing a selected kinked nanowire on top of the SU8 layer, as well as the metal alignment markers below the SU8 layer, which are used in registration of subsequent lithography steps. Scale bar, 10  $\mu$ m. **e**, Bright-field optical image of the tip end that highlights the kinked silicon nanowire and the underlying patterned SU8 probe body. Scale bar, 10  $\mu$ m. **f**, Digital camera image of a fully fabricated probe on the Ni sacrificial layer. Scale bar, 1 mm. The inset shows a bright-field optical image of the probe tip with the photoresist protection cap over the nanowire device. The photoresist protection cap is false-coloured in orange for clarity. Scale bar, 10  $\mu$ m. **g**, Schematic of the assembly of a probe onto a printed circuit board connector body (yellow and dark green). A thin Si lever support (grey) was first glued on the printed circuit board connector, and then the nanowire/SU8 probe body (light green) was aligned and attached on top. The length of the polymer probe is longer than the Si lever so that the kinked nanowire is suspended fully. For clarity, sizes are not to scale. **h**, Digital camera image of the nanowire/SU8 probe body released from the substrate after etching. Scale bar, 2 mm. **i**, Digital camera image of the fully assembled probe on the printed circuit board connector. Scale bar, 2 mm. **j**, Bright-field optical image of the suspended nanoFET probe on top of the Si lever with the photoresist protection cap. Scale bar, 100  $\mu$ m.

and a photosensitive protection cap was defined at the tip (Fig. 2c). This cap protects the nanowire tip from capillary forces and contamination during assembly to the probe body and storage prior to cell experiments. Images of a completed probe-end structure (Fig. 2f) show the overall probe structure and protection cap at the end of the wired-up nanowire tip. The probe-end structures are easily fabricated in parallel. We processed  $3 \times 4$  arrays of probes on substrates of about  $3 \times 3$  cm<sup>2</sup> (Supplementary Fig. 1), and larger arrays could be fabricated using EBL instruments capable of handling larger substrates.

To complete the probe we assembled the probe-end structure to a printed circuit board (Fig. 2g, and Supplementary Methods). A silicon microlever shorter than the nanowire/SU8 probe structure was glued to the printed circuit board, and then the probe-end structure, released by Ni underlayer etching, was removed from solution (Fig. 2h), aligned, glued and electrically connected to the microlever/printed circuit board. An image of an assembled probe (Fig. 2i) highlights the electrical connection and microlever support; a zoom of the tip region (Fig. 2j) shows the

nanowire/SU8/metal interconnect structure and protection cap of the probe end.

We used the free-standing nanowire probes alone or with a second independent probe to interrogate live cells (Fig. 3a). All measurements were carried out in an inverted microscope with probes mounted in XYZ manipulators and a temperature-regulated cell medium (Fig. 3b). Prior to measurements, the photosensitive protection cap on the end of the nanowire probe was removed in solution, and for cell measurements the nanowire end was coated with phospholipid layers, as described previously<sup>10–12</sup> (see Supplementary Methods).

A differential interference contrast image that shows the ends of a free-standing nanowire probe and patch-clamp micropipette recording from a single cultured cardiomyocyte cell (Fig. 3c) highlights the capability of targeting the nanowire probe to specific cell regions and its smaller tip size compared to a patch-clamp micropipette. The sensitivity of these nanoFET probes was characterized before and after cell measurements so that recorded conductance data could be presented as potential (millivolts) values (see

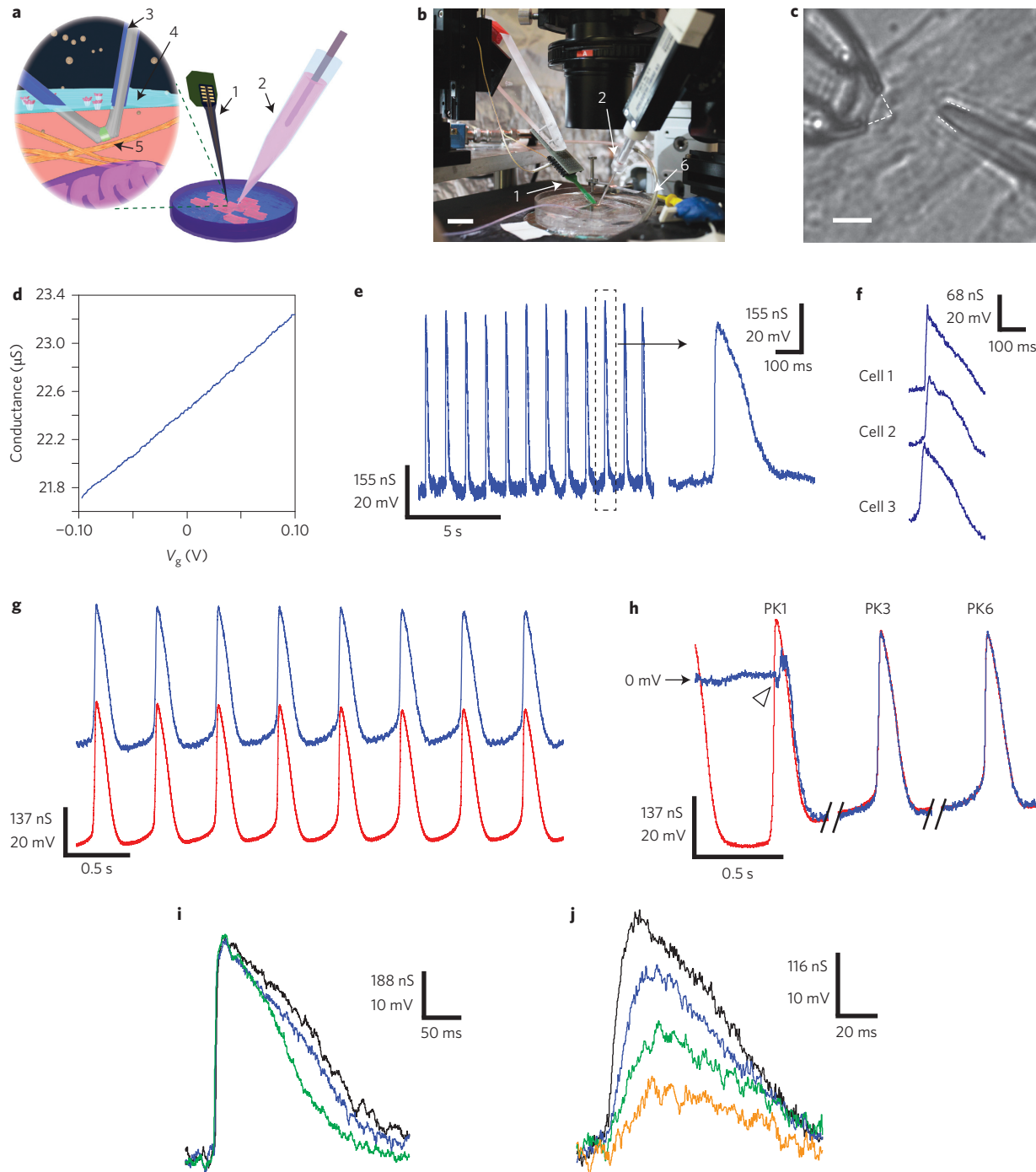


**Figure 3 | Intracellular recording using free-standing nanowire probes.** **a**, Schematic illustrating the general experiment set-up. A free-standing nanowire probe (1) is mounted on an XYZ micromanipulator to target selected cells and record IC signals, and a patch-clamp pipette (2), which is also mounted on a manipulator, can be used to monitor the same cell simultaneously. The nanowire is coated with a phospholipid layer (3) to facilitate penetration through the cell membrane (4) so that the nanoFET (5) is inside the cytoplasm. **b**, Digital camera image of the experiment set-up in which free-standing nanowire (1) and patch-clamp (2) probes are visible. An Ag/AgCl reference (water-gate) electrode (6) was used as reference. Scale bar, 2 cm. **c**, Differential interference contrast image of the kinked nanowire probe (left) and patch-clamp pipette (right) recording from the same cell. Scale bar, 5  $\mu\text{m}$ . The white dashed lines highlight the kinked nanowire and micropipette inner diameter. **d**, Conductance versus water-gate data for a typical free-standing nanowire probe recorded with source/drain voltage of 0.1 V. **e**, IC action potentials (APs) recorded from a spontaneously beating cardiomyocyte using the nanoFET probe (blue). Right: zoom-in of a single AP. **f**, Representative IC AP peaks recorded from three different cells using the same probe consecutively; the probe was not cleaned between trials. **g**, Simultaneous data recorded by a free-standing nanowire probe (blue) and patch clamp (red, current-clamp mode,  $I_{\text{clamp}} = 0$ ) from the same spontaneously beating cardiomyocyte. For clarity, signals are offset vertically. **h**, Raw signals recorded from the nanoFET probe (blue) and the patch clamp (red) as the nanoFET approaches the cell. The triangle marks the time when the nanoFET enters the cell. PK1, PK3 and PK6 mark the first, third and sixth AP peaks, respectively. **i**, IC AP peaks recorded from nanoFET at 0 s (black), 60 s (blue) and 110 s (green) after adding 10 mM nifedipine (5  $\mu\text{l}$ , DMSO solution) to the medium. **j**, IC AP peaks recorded from nanoFET at 0 s (black), 3 s (blue), 12 s (green) and 22 s (orange) after adding 1 mM TTX (1 ml, aqueous solution) to the medium.

Supplementary Methods). Representative data recorded in PBS solution (Fig. 3d) yield a sensitivity ( $7,730 \text{ nS V}^{-1}$ ) similar to previous values for chip-based kinked nanowire devices<sup>10</sup> and to the average ( $8,500 \pm 4,300 \text{ nS V}^{-1}$ ) for probes in our studies. Significantly, the variation in nanoFET sensitivities before and after cell measurements was  $<10\%$  and often only  $\sim 1\%$ , which shows that the probes provide reproducible, quantitative potential data.

Data recorded with a phospholipid-modified free-standing nanowire probe from spontaneously beating rat neonatal cardiomyocytes (Fig. 3e) exhibit regular peaks with amplitude (67 mV), duration (260 ms) and shape characteristics<sup>16,17</sup> of IC cardiac action potentials (APs). The IC AP peaks were observed 1–20 s after the phospholipid-modified nanoFET was brought into gentle contact with the cell membrane using the 40 nm step resolution of the manipulator, and they disappeared when the probe was retracted from the membrane. We were unable to record IC AP signals with unmodified nanoFET probes. These results are consistent with biomimetic membrane fusion<sup>10–13,18</sup>, and the high positioning accuracy of our free-standing probes should enable future studies of targeting and internalization with specific ligand/receptor functionalized<sup>19–21</sup> probe tips.

In addition, comparison of IC AP peaks recorded sequentially from three cells using the same nanowire probe (Fig. 3f) shows that these similar AP signals have amplitudes of 51, 46 and 56 mV for cells 1, 2 and 3, respectively. These recorded AP amplitudes are consistent with the average values determined from independent nanoFET and patch-clamp probes,  $55 \pm 16 \text{ mV}$  ( $N = 15$ ) and  $58 \pm 25 \text{ mV}$  ( $N = 13$ ), respectively, on similar cultured cardiomyocytes (DIV3). These results show that our free-standing nanowire probes can be used in multiple measurements on arrays of cells or cell networks, which could improve the efficiency of such studies compared to patch-clamp measurements where the glass pipette is replaced for each try on a new cell.

We also carried out simultaneous measurements on the same cell using both kinked nanowire and patch-clamp probes (for example, Fig. 3a,c). In these experiments, we first established IC recording with a patch clamp in the whole-cell current-clamp mode, and then brought the kinked nanowire probe into contact with the cell to establish the nanoFET IC signal. These data exhibit several key features. First, qualitative inspection of the simultaneous IC AP signals from the nanoFET and patch clamp (Fig. 3g) show that they are very similar in absolute amplitude and time-dependent shape. Second, analysis of the signal changes as the nanoFET enters the cell (Fig. 3h) reveals that there was a about a  $-50 \text{ mV}$  baseline jump as the nanoFET crosses the cell membrane (triangle, Fig. 3h), and that, after this first entry peak, all subsequent AP signals from the nanoFET and patch clamp (blue and red, respectively, Fig. 3h) overlap identically with a 65 mV peak amplitude.

A small depolarization ( $\sim 8 \text{ mV}$ ) in the resting potential of the patch clamp was observed as the nanowire probe entered the cell, which is probably because of leakage of the patch electrode membrane seal and not nanoFET leakage, as follows. First, the patch-clamp recording is sensitive to the contact between the nanoFET and cell membrane, and we have observed that touching but not penetrating cell membranes with the nanoFET can lead to depolarization and/or loss of patch-clamp signals. Second, independent single-probe experiments show that the mean stable AP recording time for the nanoFET probe, five minutes ( $N = 10$ ), is longer than that for the patch-clamp probe, 2.4 minutes ( $N = 11$ ), using the same experimental set-up. Third, extended recording with a nanoFET probe (Supplementary Fig. 2) yields full-amplitude 85 mV AP signals over a five minute period with  $<3\%$  loss of signal amplitude, and thus demonstrates a high-quality membrane seal and minimal effect on the physiological status of the cell by nanoFET insertion.

Significantly, only two parameters intrinsic to the nanoFET are used to convert probe conductance into local potential: (1) the

extracellular conductance baseline, which is assigned zero potential (black arrow, Fig. 3h), and (2) the sensitivity of the nanoFET. Hence, the agreement of both position and shape between the two traces is the first and only direct evidence to date for minimally invasive IC recording by a nanodevice. Moreover, these data clearly differentiate our nanoelectronic probes from other IC-like recordings based on high seal resistance around extracellular electrodes and localized electroporation<sup>7–9,22</sup>. In addition, the average amplitude of the APs,  $55 \pm 16 \text{ mV}$  (nanoFET,  $N = 15$ ) and  $58 \pm 25 \text{ mV}$  (patch clamp,  $N = 13$ ), and rest potentials,  $-37 \pm 10 \text{ mV}$  (nanoFET) and  $-43 \pm 13 \text{ mV}$  (patch clamp), obtained from single-probe recording experiments are indistinguishable statistically. Last, the highest amplitudes of APs reach 90 mV (Supplementary Fig. 3), which thus confirms the high quality of the nanoFET/cell membrane junctions.

Our free-standing kinked nanowire probes were also used to characterize quantitatively the effects of ion-channel blockers on recorded IC APs. First, the L-type  $\text{Ca}^{2+}$ -channel blocker nifedipine was injected into the medium after a stable IC AP recording was established from a cardiomyocyte cell. Monitoring of the nanoFET signal (Fig. 3i) shows a constant AP peak amplitude and progressive decrease in the full-width at half-maximum (FWHM) of 147, 130 and 102 ms at times 0, 60 and 110 s, respectively, after nifedipine injection. The decrease in AP peak FWHM at a constant peak amplitude is consistent with a decrease in the  $\text{Ca}^{2+}$  current caused by nifedipine binding<sup>23</sup>. Second, addition of the  $\text{Na}^+$  channel blocker tetrodotoxin (TTX) monitored in a separate experiment (Fig. 3j) shows a rapid decrease in the initial fast rising (depolarization) edge and corresponding decrease in the peak amplitude of the AP versus time. The slopes ( $\text{V s}^{-1}$ )/peak amplitudes (mV) were 3.42/44, 1.73/28, 0.78/20 and 0.53/13 for 0, 3, 12 and 22 s, respectively, after TTX addition, and are consistent with the suppression of the inward  $\text{Na}^+$  current caused by TTX binding<sup>23</sup>. These results confirm that nanoFET probes record details of IC AP changes in a reliable and robust manner, and show that they can be a tool for drug screening and cell signalling studies in the future.

Last, we explored the use of two nanoFET probes in multiplexed recording experiments. For example, two distinct nanoFET probes mounted on independent manipulators (Fig. 4a) were used to target cultured cardiomyocyte cells precisely, including two adjacent cells with well-defined alignment (Fig. 4b) and a single cell (Fig. 4c). Targeting with submicron resolution was readily achieved using differential interference contrast imaging, and could be improved further using fluorescence imaging. Representative data recorded from two nanoFET probes as they were sequentially brought into contact and internalized by two adjacent cardiomyocytes (Fig. 4d) highlight several key points. First, following gentle contact of the phospholipid-modified probes with the cell (40 nm step resolution), both probes showed a short ( $\sim 2 \text{ s}$ ) time delay before IC AP peaks appeared, and stable full-amplitude APs developed after several additional seconds. Second, the full-amplitude APs recorded with probe-1 and probe-2 (50 and 45 mV, respectively) are consistent with both independent patch-clamp measurements and the literature<sup>24</sup> for neonatal (versus adult) cardiomyocytes. The extracellular-to-IC baseline shifts can also be smaller for these neonatal cells (that is,  $-20 \text{ mV}$  for probe-2 versus  $-43 \text{ mV}$  for probe-1), but are consistent with the stage of our neonatal cell culture<sup>24</sup>. These multiplexed studies further highlight the robustness of our free-standing nanowire probe fabrication and the potential to characterize AP timing differences for precisely defined nanoprobe/cell configurations and structures too small for conventional patch-clamp measurements, such as dendritic spines<sup>25</sup>. Moreover, the capability to specify with high resolution the specific cells and/or cellular regions targeted by the nanoFET detectors represents an advantage compared to multiplexed recording with

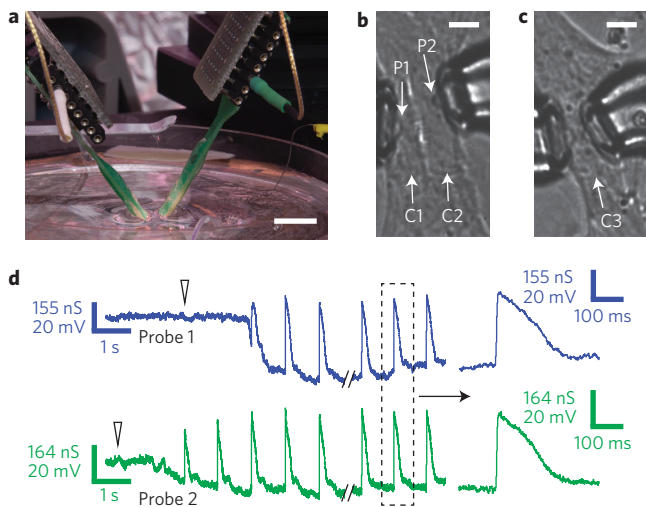


**Figure 4 | Multiplexed recording with free-standing nanowire probes.**

**a**, Digital camera image of a measurement set-up that uses two independent free-standing nanowire probes, where each probe is mounted on an independent XYZ micromanipulator. Scale bar, 1 cm. **b,c**, Differential interference contrast images of the kinked nanowire probes during multiplexed recording. Probes P1 and P2 are positioned at two adjacent cardiomyocytes C1 and C2, respectively (**b**). The two probes are positioned within submicrometre separation on the same cardiomyocyte cell, C3 (**c**). Scale bars, 10  $\mu\text{m}$ . **d**, Multiplexed IC APs recorded with the dual-kinked nanowire probe set-up from two adjacent cardiomyocytes (left). The triangles mark the time of contact between the nanowire tips and the cells. Zoom-ins of the APs marked by the dashed box are shown on the right.

nanoFET probes fabricated on planar substrates. The physical dimensions of the manipulators used for targeting nanoFET probes will limit the level of multiplexing compared to chip-based methods<sup>2,3</sup>, although future studies that incorporate kinked nanowire structures with synthetically encoded multiple nanoFET sensors<sup>26</sup> could mitigate this by increasing the number of detectors on each probe.

In summary, we have demonstrated a robust approach for the fabrication of free-standing silicon kinked nanowire probes with encoded nanoFET detectors at the tip ends. These probes were manipulated in 3D with submicron precision to target specific cells and/or cell regions and record stable full-amplitude APs from spontaneously beating cardiomyocytes. Simultaneous measurements from the same cell made with kinked nanowire and patch-clamp probes showed that the same AP amplitude and temporal properties were recorded without corrections to the raw nanowire signal, which thus demonstrates the first direct evidence for a minimally invasive, true IC recording by a nanodevice. In addition, we demonstrated real-time monitoring of AP changes as different ion-channel blockers are added to cells, and multiplexed recording from adjacent cells with precisely defined alignment and separation using two independent nanoFET probes. The signal-to-noise ratio of our single nanoFET probe ( $\sim 100$ ) is comparable to or smaller than those of vertical nanowire arrays ( $\sim 100$  (ref. 8) and  $\sim 590$  (ref. 7)), although the effective areas of these passive nanoprobe are  $>50$  times larger than our nanoFET probes. Hence, a direct comparison of signal and noise between these experiments is difficult to make because the signal and bandwidth are substantially degraded for these other devices when reduced to the same size as our current nanoFET probes.

Although future studies are needed to extend the performance and biochemical functionality of our free-standing nanowire probes, we believe this work opens up a number of interesting directions. First, our general approach for fabricating free-standing

probes could be applied to other nanoelectronic building blocks that have been used in a chip-based format<sup>11–13,26</sup>. For example, the use of U-shape kinked nanowire structures would yield ultra-small nanoFET detectors with a very high aspect ratio<sup>26</sup>, and thus enhance capabilities for specific targeting, multiplexed experiments and deep tissue/cell insertion and detection with subcellular resolution. Second, the small detector size and absence of ion exchange for our nanowire probes could facilitate studies of high-input impedance cells, such as cystic artery<sup>27</sup>, fibroblasts<sup>28</sup> and glial cells<sup>29</sup>. There are also areas in which the nanoFET probes are currently limited compared to patch-clamp technology, including the capability to stimulate APs and deliver molecular and/or macromolecular reagents. Last, we believe that our approach could be scaled up in the future to make these novel 3D nanoelectronic probes accessible to a broad range of users in electrophysiology, bioelectronics and related fields.

## Methods

Kinked silicon nanowires with nanoFETs encoded near the kink were synthesized using a gold nanocluster catalysed vapour–liquid–solid growth method as described previously<sup>15</sup>. Probe fabrication was carried out on Si substrates (Nova Electronic Materials) with 600 nm SiO<sub>2</sub> coated with 100 nm Ni, which served as relief layer, and prebaked (65 °C for two minutes) SU8 2000.5 photoresist. Kinked nanowires were deposited on the desired region from ethanol dispersion using a micropipette, and then EBL was used to define the nanowire end of the probe and PL used to pattern the remainder of the 4.5 mm long SU8 probe body, which also served as the lower passivation of metal interconnects. Subsequently, a combination of EBL and PL steps was used to define the metal connections that scale from the kinked nanowire arms to the millimetre end of the probe, where Cr/Pd/Cr (1.5/120/60 nm) was used for contacts to the nanowire, and Cr/Au (5/200 nm) for the rest of the interconnections. Top SU8 passivation/structural layers were defined using a 500 nm thick SU8 2000.5 for the tip region covering the metal contacts, and a 50  $\mu\text{m}$  thick low-stress SU8 layer (GLM 2060, Gersteltec) for the majority of the probe body, which can increase the overall mechanical strength. The kinked nanowire end of the probe was protected with 300 and 500 nm thick layers of LOR 3A and S1805 (MicroChem) defined by PL. After etching the Ni layer (40% FeCl<sub>3</sub>:39% HCl:H<sub>2</sub>O = 1:1:20), the floating probe structure was removed using tweezers and glued to the printed circuit board connector portion of the probe body mounted in the 3D manipulator. The protective cap was removed immediately prior to measurements following ultraviolet exposure, and measurements were made in a similar manner to those of previous chip-based device studies<sup>10,11</sup>. Additional fabrication details, as well as cell-culture and measurement protocols, are described in the Supplementary Information.

Received 12 August 2013; accepted 13 November 2013; published online 15 December 2013

## References

1. Parpura, V. Bionanoelectronics: getting close to the action. *Nature Nanotech.* **7**, 143–145 (2012).
2. Spira, M. & Hai, A. Multi-electrode array technologies for neuroscience and cardiology. *Nature Nanotech.* **8**, 83–94 (2013).
3. Duan, X., Fu, T.-M., Liu, J. & Lieber, C. M. Nanoelectronics–biology frontier: from nanoscopic probes for action potential recording in live cells to three-dimensional cyborg tissues. *Nano Today* **8**, 351–373 (2013).
4. Dunlop, J., Bowlby, M., Peri, R., Vasilyev, D. & Arias, R. High-throughput electrophysiology: an emerging paradigm for ion-channel screening and physiology. *Nature Rev. Drug Discov.* **7**, 358–368 (2008).
5. Molleman, A. *Patch Clamping: An Introductory Guide to Patch Clamp Electrophysiology* (Wiley, 2003).
6. Sakmann B. & Neher E. *Single-Channel Recording* (Plenum Press, 1995).
7. Xie, C., Lin, Z., Hanson, L., Cui, Y. & Cui, B. Intracellular recording of action potentials by nanopillar electroporation. *Nature Nanotech.* **7**, 185–190 (2012).
8. Robinson, J. T. *et al.* Vertical nanowire electrode arrays as a scalable platform for intracellular interfacing to neuronal circuits. *Nature Nanotech.* **7**, 180–184 (2012).
9. Hai, A., Shappir, J. & Spira, M. E. Long-term, multisite, parallel, in-cell recording and stimulation by an array of extracellular microelectrodes. *J. Neurophysiol.* **104**, 559–568 (2010).
10. Tian, B. *et al.* Three-dimensional, flexible nanoscale field-effect transistors as localized bioprobes. *Science* **329**, 830–834 (2010).
11. Jiang, Z., Qing, Q., Xie, P., Gao, R. X. & Lieber, C. M. Kinked *p–n* junction nanowire probes for high spatial resolution sensing and intracellular recording. *Nano Lett.* **12**, 1711–1716 (2012).
12. Duan, X. J. *et al.* Intracellular recordings of action potentials by an extracellular nanoscale field-effect transistor. *Nature Nanotech.* **7**, 174–179 (2012).

13. Gao, R. X. *et al.* Outside looking in: nanotube transistor intracellular sensors. *Nano Lett.* **12**, 3329–3333 (2012).
14. Tian, B. *et al.* Macroporous nanowire nanoelectronic scaffolds for synthetic tissues. *Nature Mater.* **11**, 986–994 (2012).
15. Tian, B., Xie, P., Kempa, T. J., Bell, D. C. & Lieber, C. M. Single-crystalline kinked semiconductor nanowire superstructures. *Nature Nanotech.* **4**, 824–829 (2009).
16. Bers, D. M. Cardiac excitation–contraction coupling. *Nature* **415**, 198–205 (2002).
17. Zipes, D. P. & Jalife, J. *Cardiac Electrophysiology: From Cell to Bedside* 2nd edn (Saunders, 2009).
18. Chernomordik, L. V. & Kozlov, M. M. Mechanics of membrane fusion. *Nature Struct. Mol. Biol.* **15**, 675–683 (2008).
19. Nicolas, J., Mura, S., Brambilla, D., Mackiewicz, N. & Couvreur, P. Design, functionalization strategies and biomedical applications of targeted biodegradable/biocompatible polymer-based nanocarriers for drug delivery. *Chem. Soc. Rev.* **42**, 1147–1235 (2013).
20. Subbiah, R., Veerapandian, M., & Yun, K. S. Nanoparticles: functionalization and multifunctional applications in biomedical sciences. *Curr. Med. Chem.* **17**, 4559–4577 (2010).
21. Kotov, N. A. *et al.* Nanomaterials for neural interfaces. *Adv. Mater.* **21**, 3970–4004 (2009).
22. Hai, A., Shappir, J. & Spira, M. E. In-cell recordings by extracellular microelectrodes. *Nature Methods* **7**, 200–202 (2010).
23. Szentandrássy, N. *et al.* Powerful technique to test selectivity of agents acting on cardiac ion channels: the action potential voltage-clamp. *Curr. Med. Chem.* **18**, 3737–3756 (2011).
24. Viatchenko-Karpinski, S. *et al.* Intracellular Ca<sup>2+</sup> oscillations drive spontaneous contractions in cardiomyocytes during early development. *Proc. Natl Acad. Sci. USA* **96**, 8259–8264 (1999).
25. Davie, J. T. *et al.* Dendritic patch-clamp recording. *Nature Protocols* **1**, 1235–1247 (2006).
26. Xu, L. *et al.* Design and synthesis of diverse functional kinked nanowire structures for nanoelectronic bioprobes. *Nano Lett.* **13**, 746–751 (2013).
27. Akbarali, H. I., Wyse, D. G. & Giles, W. R. Ionic currents in single cells from human cystic artery. *Circ. Res.* **70**, 536–545 (1992).
28. Chilton, L. *et al.* K<sup>+</sup> currents regulate the resting membrane potential, proliferation, and contractile responses in ventricular fibroblasts and myofibroblasts. *Am. J. Physiol. Heart Circ. Physiol.* **288**, H2931–H2939 (2005).
29. Clark, B. A. & Mobbs, P. Voltage-gated currents in rabbit retinal astrocytes. *Eur. J. Neurosci.* **6**, 1406–1414 (1994).

### Acknowledgements

C.M.L. acknowledges support of this work by a National Institutes of Health Director's Pioneer Award (5DP1OD003900), National Basic Research Program of China (2013CB934103), and International Science & Technology Corporation Program of China (2013DFA50840).

### Author contributions

Q.Q., Z.J. and C.M.L. designed the experiments, Q.Q., Z.J., and L.X. performed the experiments, R.G. helped in cardiomyocyte culture experiments, Q.Q., Z.J., L.X. and C.M.L. analysed data and Q.Q., Z.J. and C.M.L. wrote the paper. All authors discussed the results and commented on the manuscript.

### Additional information

Supplementary information is available in the [online version](#) of the paper. Reprints and permissions information is available online at [www.nature.com/reprints](http://www.nature.com/reprints). Correspondence and requests for materials should be addressed to C.M.L.

### Competing financial interests

The authors declare no competing financial interests.